Conductivity of graphene with resonant and non-resonant adsorbates

Guy Trambly de Laissardière, Didier Mayou

Conductivity of graphene with resonant and non resonant adsorbates

Guy Trambly de Laissardière[1] and Didier Mayou[2]

[1] *Laboratoire de Physique théorique et Modélisation, CNRS and Université de Cergy-Pontoise, 95302 Cergy-Pontoise, France*

[2] *Univ. Grenoble Alpes, Inst NEEL, F-38042 Grenoble, France CNRS, Inst NEEL, F-38042 Grenoble, France*

(Dated: November 27, 2013)

We propose a unified description of transport in graphene with adsorbates that fully takes into account localization effects and loss of electronic coherence due to inelastic processes. We focus in particular on the role of the scattering properties of the adsorbates and analyze in detail cases with resonant or non resonant scattering. For both models we identify several regimes of conduction depending on the value of the Fermi energy. Sufficiently far from the Dirac energy and at sufficiently small concentrations the semi-classical theory can be a good approximation. Near the Dirac energy we identify different quantum regimes, where the conductivity presents universal behaviors.

PACS numbers: 72.15.Rn, 73.20.Hb, 72.80.Vp, 73.23.-b,

Electronic transport in graphene [1–4] is sensitive to static defects that are for example frozen ripples, screened charged impurities, or local defects like vacancies or adsorbates [5–8]. Adsorbates, which can be organic groups or adatoms attached to the surface of graphene, are of particular interest in the context of functionalisation which aims at controlling the electronic properties by attaching atoms or molecules to graphene [9–14]. Therefore there is a need for a theory of conductivity in the presence of such defects.

Theoretical studies of transport in the presence of local defects have dealt mainly either with the Bloch-Boltzmann formalism or with self-consistent approximations [10, 15–22]. In these theories a major length scale that characterizes the electron scattering is the elastic mean-free path L_e. These approaches indeed explain some experimental observations such as the quasilinear variation of conductivity with concentration of charge carriers [10–14]. Yet these theories have important limitations and can hardly describe in detail the localization phenomena that has been reported in some experiments [6, 7, 11, 12]. Indeed in the presence of a short range potential, such as that produced by local defects the electronic states are localized on a length scale ξ [23–26]. A sample will be insulating unless some source of scattering, like electron-electron or electron-phonon interaction, leads to a loss of the phase coherence on a length scale $L_i < \xi$. Therefore, in addition to the elastic mean-free path L_e, the inelastic mean-free path L_i and the localization length ξ play also a fundamental role for the conductivity of graphene with adsorbates.

In this letter we develop a numerical approach for the conductivity that treats exactly the tight-binding Hamiltonian and takes fully into account the effect of Anderson localization. This approach gives access to the characteristic lengths and to the conductivity as a function of the concentration, the Fermi energy $E_{\rm F}$ and the inelastic mean-free path L_i. In real samples L_i depends on the temperature, or magnetic field, but it is an adjustable parameter in this work. Our results confirm that sufficiently far from the Dirac energy, and for sufficiently small adsorbates concentrations, the Bloch-Boltzmann theory and the self-consistent theories are valid when $L_e \ll L_i \ll \xi$. Near the Dirac energy we identify different regimes of transport that depend on whether the adsorbates produce resonant or non resonant scattering. These different regimes of transport present some universal characteristics which consequences are discussed for experimental measurements of conductivity and magneto-conductivity.

Models of adsorbates

The scattering properties of local defects like adsorbates or vacancies is characterized by their T-matrix. Local defects tend to scatter electrons in an isotropic way for each valley and lead also to strong inter valley scattering. Yet the energy dependence of the T-matrix depends very much on the type of defect and in this work we focus on the role of this energy dependence. To this end we consider two models for which the T-matrix diverges at the Dirac energy (resonant adsorbates leading to mid-gap states also called zero energy modes) or is constant (non resonant adsorbates). Note that resonances can occur also at non zero energy but here we restrict to the important case of zero energy modes. The conclusions drawn here, concerning the influence of the energy dependence of the T-matrix for adsorbates, are useful for other types of local defects.

We consider that the adsorbates create a covalent bond with some atoms of the graphene sheet. Then a generic model is obtained by removing the p_z orbitals of these carbon atoms [17–19, 22–29]. For example an hydrogen adsorbate can be modeled by removing the p_z orbital of the carbon atom that is just below the hydrogen atom. This is the model of resonant adsorbate that we consider here. In this case the T-matrix associated to the adsorbate, diverges at the Dirac energy hence the name of resonant scatterers. The non resonant model is consti-

tuted by two neighboring missing orbitals (divacancy). In that case the T-matrix is nearly constant close to the Dirac energy and does not diverge.

Finally we consider here that the up and down spin are degenerate i.e. we deal with a paramagnetic state. Indeed the existence of a magnetic state for various adsorbates, like hydrogen for example, is still debated [30]. Let us emphasize that in the case of a magnetic state the up and down spin give two different contributions to the conductivity but the individual contribution of each spin can be analyzed from the results discussed here. With these assumptions the generic model Hamiltonian for adsorbates writes:

$$H = -t \sum_{\langle i,j \rangle} (c_i^+ c_j + c_j^+ c_i) \qquad (1)$$

where $\langle i,j \rangle$ represents nearest neighbours pairs of occupied sites and $t = 2.7\,\mathrm{eV}$ determines the energy scale. In our calculations the vacant sites (resonant adsorbates) or the di-vacant sites (non resonant adsorbates) are distributed at random with a finite concentration.

Evaluation of the conductivity

The present study relies upon the Einstein relation between the conductivity and the quantum diffusion. We evaluate numerically the quantum diffusion using the MKRT approach [31–35]. This method has been used to study quantum transport in disordered graphene, chemically doped graphene, graphene with functionalization and graphene with structural defects [13, 14, 26, 29, 36–41]. We introduce an inelastic scattering time τ_i, beyond which the propagation becomes diffusive due to the destruction of coherence by inelastic processes (relaxation time approximation) [42–47]. We finally get (Supplemental Material Sec. I):

$$\sigma(E_\mathrm{F}, \tau_i) = e^2 n(E_\mathrm{F}) D(E_\mathrm{F}, \tau_i) \qquad (2)$$

$$D(E_\mathrm{F}, \tau_i) = \frac{L_i^2(E_\mathrm{F}, \tau_i)}{2\tau_i} \qquad (3)$$

where E_F is the Fermi energy, $n(E_\mathrm{F})$ the density of states (DOS), $D(E_\mathrm{F}, \tau_i)$ the diffusivity, τ_i the inelastic scattering time and $L_i(E_\mathrm{F}, \tau_i)$ the inelastic mean-free path. $L_i(E_\mathrm{F}, \tau_i)$ is the typical distance of propagation during the time interval τ_i for electrons at the energy E_F in the system without inelastic scattering [48].

The typical variation of $\sigma(\tau_i)$ in our study (Supplemental Material Sec. II) is equivalent to that found in previous works [14, 38]. At small times the propagation is ballistic and the conductivity $\sigma(\tau_i)$ increases when τ_i increases. For large τ_i the conductivity $\sigma(\tau_i)$ decreases with increasing τ_i due to quantum interferences effects and ultimately goes to zero in our case due to Anderson localization in 2 dimension.

We define the microscopic conductivity σ_M as the maximum value of the conductivity over all values of τ_i. According to the renormalization theory this value is obtained when the inelastic mean-free path $L_i(\tau_i)$ and the elastic mean-free path L_e are comparable. This microscopic conductivity σ_M represents the conductivity without the effect of quantum interferences in the diffusive regime (localization effects) and can be compared to semi-classical or self-consistent theories which also do not take into account the effect of quantum interferences in the diffusive regime.

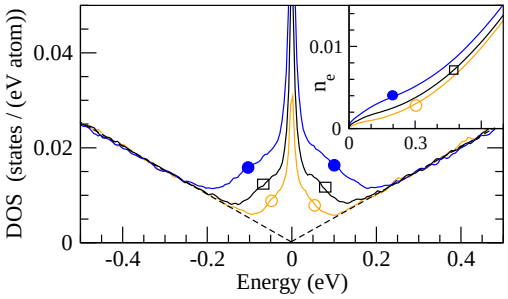

FIG. 1: Densities of states versus energy for resonant adsorbates (monovacancies) with concentrations (empty circles) 0.1%, (empty square) 0.2%, (filled circle) 0.4%. (Dashed lines) without adsorbate. [Inset: electron density per atom n_e versus energy.]

Finally we note that in the above formulas it is assumed that the inelastic scattering does not affect the DOS $n(E_\mathrm{F})$. However this scattering can lead also to a mixing of states that affects the DOS. In the Supplemental Material (Sec. V) we analyze in detail this effect of mixing of states. Although it is difficult to quantify our results strongly suggest that the effect of the mixing plays a minor role except for the microscopic conductivity σ_M of the zero energy modes where indeed the DOS varies quickly. This leads us to conclusions in contrast with those of a recent study [26] (see below and Supplemental Material Sec. V).

Resonant adsorbates (monovacancies)

Figure 1 shows the total DOS with three different regimes consistent with previous studies [10, 26]. At sufficiently large energies the density of pure graphene is weakly affected. Near the Dirac energy there is an intermediate regime where the pseudo-gap is filled. Very close to the Dirac point there is a third regime where the density presents a peak which is reminiscent of the mid-gap state (also called zero energy modes) produced by just one missing orbital.

Figure 2 shows these three regimes for the microscopic conductivity σ_M. In the first regime i.e. at sufficiently large energies, $\sigma_M \simeq \sigma_\mathrm{B}$, where σ_B is calculated with the Bloch-Boltzmann approach [19]. In this regime where the DOS is weakly affected (see above), $\sigma_M \gg G_0 = 2e^2/h$ and $\xi \gg L_e$ (Supplemental Material Sec. III and IV).

When the energy decreases, the semi-classical model fails (figure 2), and a second regime occurs in which $\sigma_M \simeq 4e^2/\pi h$. This is consistent with predictions of

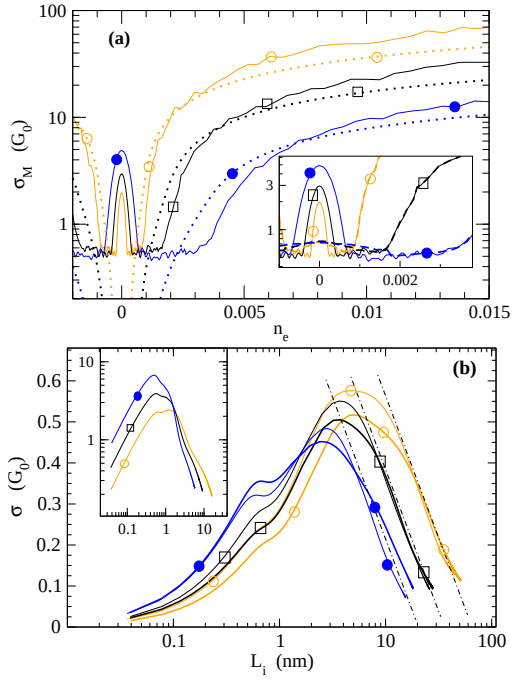

FIG. 2: Conductivity for resonant adsorbates (monovacancies) for 3 concentrations (see caption of figure 1). (a) Microscopic conductivity σ_M versus electron density per atom n_e. (Dotted lines) predictions of the Boltzmann theory close to the Dirac energy [19]. [Inset: zoom on the low concentration limit: (lines) without mixing of states, (dashed lines) with mixing of states on an energy range $\delta E = \hbar/\tau_i$ (Supplemental Material Sec. V).] (b) Conductivity σ versus inelastic scattering length L_i at energies $E = 0.03\,\text{eV}$ (thin line), and $E = 0.04\,\text{eV}$ (thick line). The dot-dashed straight lines show the slope $\alpha = 0.25$ for $L_i \gg L_e$ (see text): [Inset: $\sigma(L_i)$ at $E = 0$ in a Log-Log scale.] $G_0 = 2e^2/h$.

self-consistent theories and with numerical calculations [10, 15–19, 22, 26]. In agreement with the literature we find that the onset for this regime corresponds to about one electron per impurity as shown by figure 2. Also this intermediate regime occurs when the Fermi wave-vector k_F is such that $k_F L_e \simeq 1$.

A characteristic length scale in this intermediate regime is the distance d between adsorbates (Supplemental Material). Here $d = 1/\sqrt{n}$ where n is the adsorbates density and $d \simeq 5\,\text{nm}$ for a concentration of 0.1%. In this intermediate regime L_e (defined precisely in the Supplemental Material Sec. III) depends on the energy but stays comparable to d. This can be understood by noting that L_e, which according to the semi-classical theory tends to zero at the Dirac energy, cannot be much smaller than the distance d between the scattering centers.

At smaller energies a peak of the microscopic conductivity σ_M appears very close to the Dirac energy which coincides with the peak of the DOS and represents a third regime of transport. This peak of conductivity is not predicted by self-consistent theories. It is not obtained by [18, 19] and is present in the calculation of [22] although much less marked than in the present work. This peak is obtained with very similar values in the recent work [26]. In this peak σ_M increases with the concentration of defects. Yet σ_M is calculated here by neglecting the mixing of energy levels due to the inelastic scattering processes. As shown in the inset of figure 2a we find that this peak can decrease when the mixing of the levels due to the inelastic scattering processes is taken into account (Supplemental Material Sec. V).

We discuss now these three regimes for the conductivity when $L_i > L_e$ (figure 2b). At high energies we find standard localization effects consistent with very large localization lengths (Supplemental Material). In the intermediate regime (i.e. $\sigma_M \simeq 4e^2/\pi h$), for concentration 0.1% to 10%, the conductivity is well represented by the equation:

$$\sigma(L_i) \simeq \frac{4e^2}{\pi h} - \alpha \frac{2e^2}{h} \text{Log}\left(\frac{L_i}{L_e}\right). \qquad (4)$$

The coefficient is $\alpha \simeq 0.25$ which is close to the result of the perturbation theory of 2 dimension Anderson localization for which $\alpha \simeq 1/\pi$ [48]. We emphasize that the regime is not perturbative close to the Dirac point. This expression shows no effect of anti localization [49] as expected for purely short range scattering. Indeed in that case graphene belongs to an orthogonal symmetry class with localization effects as in standard 2 dimension metal without spin-orbit coupling [50]. The localization length ξ deduced from this expression (4) is such that $\sigma(\xi) = 0$ which gives $\xi \simeq 13 L_e$. This results justifies previous estimates of the localization length from the calculation of the elastic mean-free path that were done in this plateau of microcopic conductivity [40]. As discussed above the elastic mean-free path L_e depends on the energy in this regime but is of the order of the distance d between adsorbates. Therefore d determines the order of magnitude of the localization length ξ and of the elastic mean-free path L_e. More precisely in the range of concentration 0.1% to 10% (Supplemental Material Sec. IV) the localization length in this regime is $\xi \simeq 20 d/r$ where the ratio r decreases with increasing energy and is $1 \leq r \leq 3$. The values of the localization length found at 10% in [24] are consistent with our study.

In the third regime where the DOS and σ_M present a peak, the conductivity does not follow the above law (equation (4)). $\sigma(L_i)$ fits better with a power law $\sigma(L_i) \propto L_i^{-\beta}$ where β depends on the concentration (here $1 < \beta < 2$). This is consistent with the divergence of the localization length ξ predicted in [23] although we do not recover the behavior found precisely at the Dirac energy. Since our energy resolution is of the order of $10^{-2}\,\text{eV}$, we conclude that the zero energy behavior of the conductance exists only in a narrow energy range and could be difficult to observe experimentally.

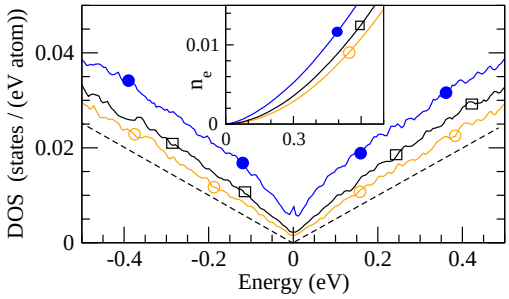

FIG. 3: Densities of states versus energy for non resonant adsorbates (divacancies) with concentrations 0.5% (empty circles), 1% (empty squares), 2% (filled circle). (Dashed lines) without adsorbate. [Inset: electron density per atom n_e versus energy.]

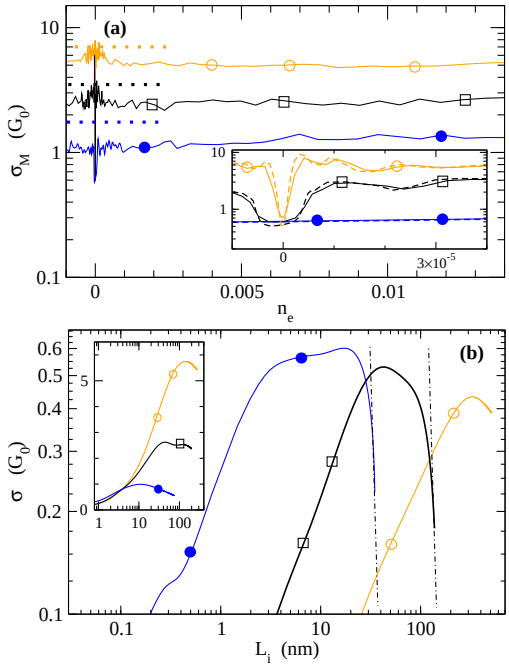

FIG. 4: Conductivity for non resonant adsorbates (divacancies) for 3 concentrations (see caption of figure 3). (a) Microscopic conductivity σ_M versus electron density per atom n_e. (Dotted lines) predictions of the Boltzmann theory close to the Dirac energy. [Inset: zoom on the low concentration limit: (lines) without mixing of states, (dashed lines) with mixing of states on an energy range $\delta E = \hbar/\tau_i$ (Supplemental Material Sec. V).] (b) Conductivity σ versus inelastic scattering length L_i at $E = 0$ in a Log-Log scale. [Inset: $\sigma(L_i)$ at $E = 0.1$ eV.] $G_0 = 2e^2/h$.

In the presence of a magnetic field the magnetic length $L(B) = \sqrt{\hbar/eB}$ plays the role of a finite coherence length just as the inelastic mean-free path $L_i(T)$. When $L(B) < L_i(T)$ the relevant coherence length is $L(B)$ and the conductivity is $\sigma(L(B))$. This could be compared to our results, in particular for equation (4).

Non resonant adsorbates (divacancies)

Figure 3 shows the total densities of states as a function of energy for the non resonant adsorbates. The result is similar to that obtained by the self-consistent Born approximation (SCBA) for Anderson disorder [15]. The two models are not strictly equivalent but have both an energy independent T-matrix close to the Dirac energy. The microscopic conductivity σ_M presents a minimum with $\sigma_M \simeq 4e^2/\pi h$ in a narrow concentration range (figure 4). Again this is consistent with the SCBA predictions for the Anderson model [15]. At the Dirac energy we find that the conductivity can be represented by a power law $\sigma(L_i) \propto L_i^{-\gamma}$ with $\gamma \simeq 4-6$. Yet the equation (4) fits also with $\alpha \simeq 0.75$ which gives $\xi \simeq 2.5 L_e$. In any case the quick decrease of the conductivity $\sigma(L_i)$ with L_i and the narrow concentration range for the minimum of σ_M suggest that the value $\sigma_M \simeq 4e^2/\pi h$ could be very difficult to find experimentally.

A recent experimental work [51] shows that graphene with defects induced by helium ion, at about 1% concentration, presents Anderson localization even at room temperature. Our study suggest that at such concentration only resonant adsorbates can create the strong localization. The length of the samples, less than 100 nm, is also consistent with small inelastic scattering [6].

Conclusion

To conclude our study shows that the energy dependence of the scattering properties of local defects is determinant for transport and magneto transport properties of graphene with adsorbates. Sufficiently far from the Dirac energy, and for not too high concentrations, the semi-classical approach is usually valid. Yet closer from the Dirac point there are regimes where the quantum effects are essential. For resonant adsorbates we find that in the regime of the so-called minimum conductivity the conductivity is well represented by equation (4). The characteristic length scale is the distance d between defects and the localization length ξ and the elastic mean-free path L_e are given by $\xi \simeq 13 L_e \simeq 20 d/r$ where the ratio r decreases with increasing energy and is $1 \leq r \leq 3$. Closer from the Dirac energy there is a peak in the DOS which corresponds to another regime of transport in a band of mid-gap states. We find a critical behaviour partly consistent with [23, 26]. In this regime we have shown that the inelastic scattering can destroy the peak of DOS, which strongly affects the conductivity. Yet a proper understanding of the physics of transport in this peak requires clearly further studies [52]. For non resonant adsorbates, in a narrow energy range near the Dirac energy the microscopic conductivity σ_M presents a minimum with the universal value $\sigma_M \simeq 4e^2/\pi h$. Yet at the Dirac energy there are strong localization effects. These could make the experimental observation of the the universal value $\sigma_M \simeq 4e^2/\pi h$ very difficult. Finally we emphasize that the methodology used here to study quantum effects for electronic transport is of wide applicability. In particular important related problems such as magneto-conductivity of graphene beyond low field limit

or competition between scattering by defects with long range and short range potential could be studied as well [49].

Acknowledgements

We thank L. Magaud, C. Berger and W. A. de Heer for fruitfull discussions and comments. The computations have been performed at the Centre de Calcul of the Université de Cergy-Pontoise. We thank Y. Costes and D. Domergue for computing assistance.

Supplemental Material

I. EVALUATION OF THE KUBO-GREENWOOD CONDUCTIVITY

The present study relies upon the evaluation of the Kubo-Greenwood conductivity using the Einstein relation between the conductivity and the quantum diffusion (see Refs. [46, 53] and Refs. therein). A central quantities are the velocity correlation function of states of energy E at time t,

$$C(E,t) = \left\langle \hat{V}_x(t)\hat{V}_x(0) + \hat{V}_x(0)\hat{V}_x(t) \right\rangle_E \quad (5)$$

$$= 2\,\mathrm{Re}\left\langle \hat{V}_x(t)\hat{V}_x(0) \right\rangle_E , \quad (6)$$

and the average square spreading (quantum diffusion) of states of energy E at time t along the x direction,

$$X^2(E,t) = \left\langle (\hat{X}(t) - \hat{X}(0)^2 \right\rangle_E . \quad (7)$$

In equations (6) and (7), $\langle ... \rangle_E$ is the average on states with energy E, Re A is the real part of A, $\hat{V}_x(t)$ and $\hat{X}(t)$ are the Heisenberg representation of the velocity operator $\hat{V}_x$ and the position operator $\hat{X}$ along x direction at time t,

$$\hat{V}_x = \frac{1}{i\hbar}\left[\hat{X}, \hat{H}\right]. \quad (8)$$

$C(E,t)$ is related to quantum diffusion by the relation [46],

$$\frac{\mathrm{d}}{\mathrm{d}t}\Big(X^2(E,t)\Big) = \int_0^t C(E,t')\mathrm{d}t'. \quad (9)$$

From Kubo-Greenwood formula, the conductivity is given by the Einstein relation,

$$\sigma(E_\mathrm{F}) = e^2 n(E_\mathrm{F}) D(E_\mathrm{F}), \quad (10)$$

where e is the electron charge, E_F the Fermi energy, n the density of states and D the diffusivity related to the square spreading by the relation [53],

$$D(E_\mathrm{F}) = \frac{1}{2}\lim_{t\to\infty}\frac{\mathrm{d}}{\mathrm{d}t}X^2(E_\mathrm{F},t). \quad (11)$$

We evaluate numerically the quantum diffusion $X^2(E,t)$ of states of energy E for the Hamiltonian using the MKRT approach [31–35]. This method allows very efficient numerical calculations by recursion in real-space. Our calculations are performed on samples containing up to 10^8 atoms which corresponds to a typical size of about one micron square. This allows to study systems with characteristic inelastic mean-free path L_i of the order of a few hundreds nanometers. With characteristic lengths of such size it is possible to treat systems with low concentrations of adsorbates that are of $0.1\%, 0.2\%, 0.4\%$ for resonant adsorbates (monovacancies) and of $0.5\%, 1\%, 2\%$ for non-resonant adsorbates (divacancies). For the results presented here the energy resolution is of the order of $10^{-2}\,\mathrm{eV}$.

The effect of the inelastic scattering is treated in a phenomenological way. This relaxation time approximation (RTA) has been used succesfully to compute [42] conductivity in approximants of Quasicrystal where quantum diffusion and localization effect play a essential role [43–45] and conductivity in organic semiconductors [47]. Following previous works [42, 46, 47, 53], we assume that the velocity correlation function $C_i(E,t)$ of the system with inelastic scattering is given by,

$$C_i(E,t) \simeq C(E,t)\,\mathrm{e}^{-|t|/\tau_i}, \quad (12)$$

where $C(E,t)$ is the velocity correlation of the system with elastic scattering (monovacancies or divacancies) but without inelastic scattering. Here the inelastic scattering time τ_i is the cutoff time of the weak localization effects also called dephasing time. As shown in Refs. [42, 46, 47, 53] the propagation given by this formalism is unaffected by inelastic scattering at short times ($t < \tau_i$) and diffusive at long times ($t > \tau_i$) as it must be. Using the $t = 0$ conditions, $X^2(E, t = 0) = 0$ and $\frac{\mathrm{d}}{\mathrm{d}t}X^2(E, t = 0) = 0$, and performing two integrations by part, we obtain from equations (9), (10), (11) and (12), [53]

$$\sigma(E_\mathrm{F},\tau_i) = e^2 n(E_\mathrm{F}) D(E_\mathrm{F},\tau_i), \quad (13)$$

$$D(E_\mathrm{F},\tau_i) = \frac{L_i^2(E_\mathrm{F},\tau_i)}{2\tau_i}, \quad (14)$$

$$L_i^2(E_\mathrm{F},\tau_i) = \frac{1}{\tau_i}\int_0^\infty X^2(E_\mathrm{F},t)\,\mathrm{e}^{-t/\tau_i}\,\mathrm{d}t, \quad (15)$$

where $L_i(E_\mathrm{F},\tau_i)$ the inelastic mean-free path and $D(E_\mathrm{F},\tau_i)$ the diffusivity. $X^2(E,t)$ is calculated for the system with the Hamiltonian given in the main text which represents only elastic scattering due to monovacancies or divacancies. The above equations treat the inelastic scattering in a way that is equivalent to the standard approximation in mesoscopic physics. Indeed, in the presence of inelastic scattering, it is usually assumed that, $L_i^2(E_\mathrm{F}) \simeq \sqrt{X^2(E_\mathrm{F},\tau_i)}$, thus the conductivity is given by the Einstein formula with a diffusivity $D(E_\mathrm{F},\tau_i) \simeq X^2(E_\mathrm{F},\tau_i)/(2\tau_i)$ [48], which is essentially equivalent to the above equations.

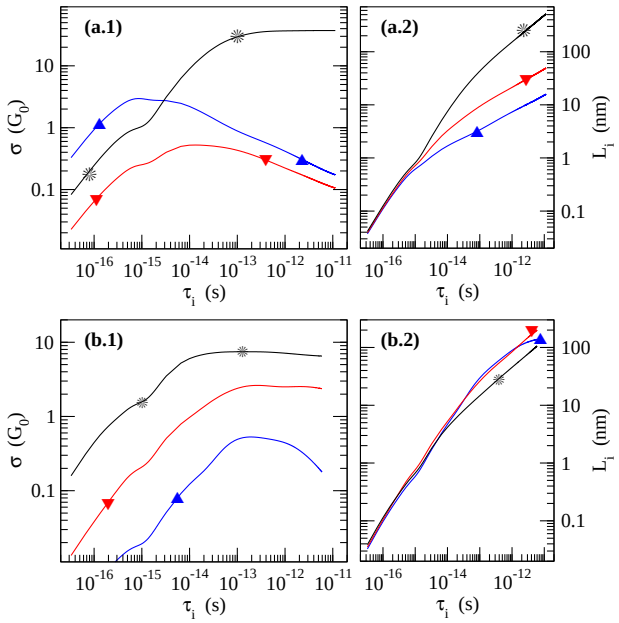

FIG. 5: Conductivity $\sigma(E,\tau_i)$ and inelastic mean-free path $L_i(E,\tau_i)$ versus inelastic scattering time τ_i. (a) Concentration 0.2% of resonant adsorbates (monovacancies) for energies $E = 0$ (triangle up), $E = 0.04\,\mathrm{eV}$ (triangle down) and $E = 0.8\,\mathrm{eV}$ (star). (b) Concentration 1% of non resonant adsorbates (divacancies) for energies $E = 0$ (triangle up), $E = 0.1\,\mathrm{eV}$ (triangle down) and $E = 1.5\,\mathrm{eV}$ (star). $G_0 = 2e^2/h$.

II. CONDUCTIVITY AND COHERENCE LENGTH VERSUS INELASTIC MEAN-FREE TIME

As explained in the main text we introduce an inelastic scattering time τ_i, beyond which the propagation becomes diffusive due to the destruction of coherence by inelastic processes. Figure 5 presents the conductivity $\sigma(E,\tau_i)$ and the inelastic mean-free path $L_i(E,\tau_i)$ calculated as a function of inelastic scattering time τ_i for different energies E. Here $L_i(E,\tau_i)$ is the length beyond which the propagation becomes diffusive due to the destruction of coherence by inelastic processes (equations (13) and (15)). Conductivities are calculated for large values of τ_i up to a few $10^{-11}\,\mathrm{s}$ which corresponds to inelastic mean-free paths up to several hundred nanometers. This is possible because we can treat large systems containing up to 10^8 atoms. We have checked the convergence of our calculations with respect to the size of the sample.

At small times the propagation is ballistic and the conductivity $\sigma(\tau_i)$ increases when τ_i increases. For large τ_i the conductivity $\sigma(\tau_i)$ decreases with increasing τ_i due to quantum interferences effects and ultimately goes to zero in our case due to Anderson localization in 2 dimension.

We define the microscopic conductivity σ_M as the maximum value of the conductivity over all values of τ_i. Ac-

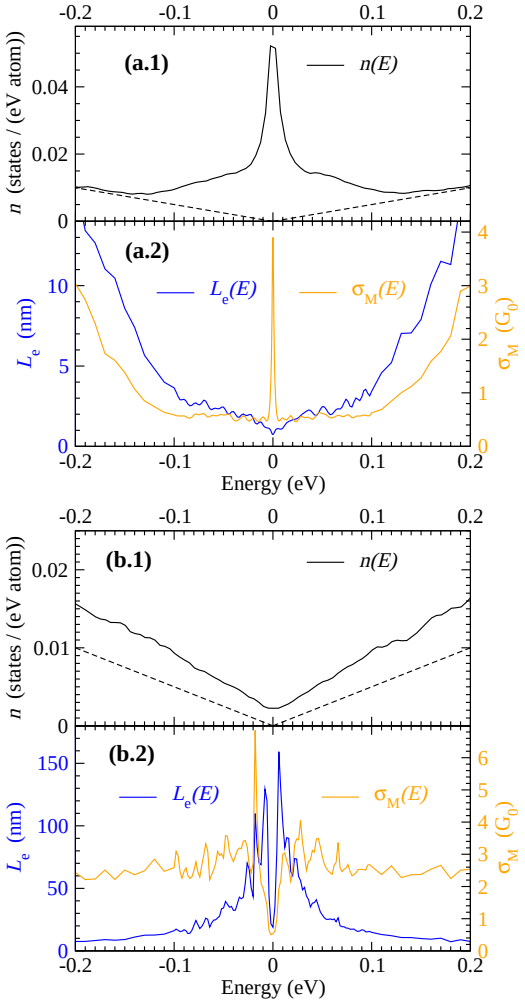

FIG. 6: Density of states n, elastic mean-free path L_e and microscopic conductivity σ_M versus energy E. (a) Concentration 0.2% of resonant adsorbates (monovacancies). (b) Concentration 1% of non resonant adsorbates (divacancies). (dashed lines) density of states of pure graphene. The elastic mean-free path is computed from the maximum of the diffusivity $D_M(\tau_i)$ by $L_e = 2D_M/V_F$, with Fermi velocity $V_F = 10^6\,\mathrm{m.s^{-1}}$. $G_0 = 2e^2/h$.

cording to the renormalization theory this value is obtained when the inelastic mean-free path $L_i(\tau_i)$ and the elastic mean-free path L_e are comparable. This microscopic conductivity σ_M represents the conductivity without the effect of quantum interferences in the diffusive regime (localization effects). Therefore σ_M be compared to semi-classical or self-consistent theories which also do not take into account the effect of quantum interferences in the diffusive regime.

III. ELASTIC MEAN-FREE PATH

We define the elastic mean-free path as $L_e = 2D_M/V_F$ where D_M is the microscopic diffusivity and V_F the Fermi

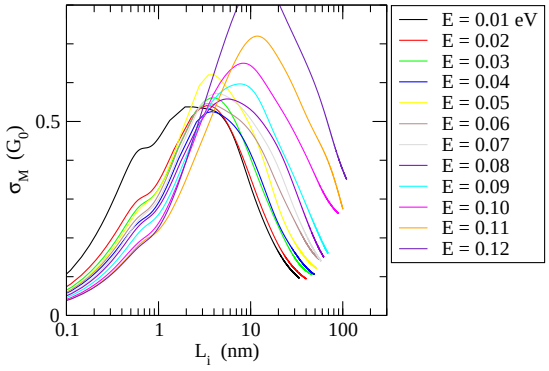

FIG. 7: Conductivity σ in unit of $G_0 = 2e^2/h$ as a function of inelastic scattering length L_i for 0.2% of resonant adsorbates (monovacancies) at various energies E.

velocity. In figure 6 we give two typical results for monovacancies and divacancies for the variation the elastic mean-free path with energy.

For 0.2% of resonant adsorbates (monovacancies) the mean-free path decreases with energy up to $E \simeq 0.1\,\mathrm{eV}$ which is the onset of the plateau of the microscopic conductivity. At $E = 0.1\,\mathrm{eV}$, L_e is of the order of 4 nm which is comparable to the distance between defects $d \simeq 3.5\,\mathrm{nm}$. When the energy decreases the mean-free path decreases also but stays of the same order and does not go to zero as predicted by the semi-classical theory. A qualitative explaination is that the elastic mean-free path cannot be much smaller than the distance between the scattering centers. This behavior is obtained at all the concentrations that we have studied. We find that, for energies in the intermediate regime (plateau of the microscopic conductivity), the elastic mean-free path is of the order of $L_e \simeq 3d/2r$ where the ratio r decreases with increasing energy and varies in the range $r = 1 - 3$.

For 1% of non resonant adsorbates (divacancies) the microscopic conductivity is essentially constant at high energies in agreement with the semi-classical and self-consistent theories. In this regime the elastic mean-free path varies roughly like the inverse of the energy. Yet close to the Dirac energy the mean-free path abruptly decreases just as the microscopic conductivity. This is in agreement with the self-consistent theory of Anderson disorder [15] that predicts an abrupt decrease of conductivity in a region where the density of states does not vary much. This means that the microscopic diffusivity D_M varies quickly and therefore the mean-free path $L_e = 2D_M/V_\mathrm{F}$ varies also quickly.

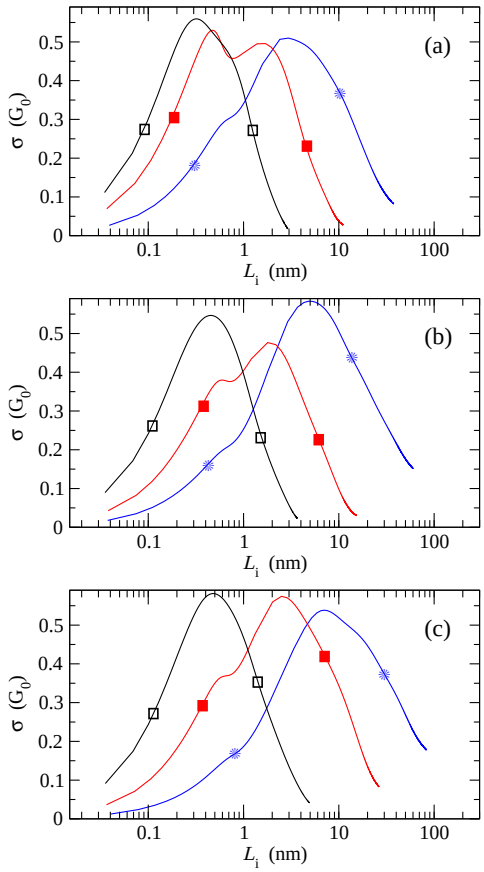

FIG. 8: Conductivity σ in unit of $G_0 = 2e^2/h$ as a function of inelastic scattering length L_i for (empty square) 0.1%, (filled square) 1%, (star) 10% of resonant adsorbates (monovacancies) at energies: (a) minimum energy of the intermediate regime, (b) middle energy the intermediate regime, (c) maximum energy of the intermediate regime.

IV. INTERMEDIATE REGIME FOR MONO VACANCIES: EFFECT OF LOCALIZATION ON THE CONDUCTIVITY

In the intermediate regime of monovacancies the microscopic conductivity σ_M is of the order of $4e^2/\pi h$. We find a universal law for the conductivity as a function the inelastic mean-free path L_i and the elastic mean-free path L_e with $L_i > L_e$ (see main text equation (4)):

$$\sigma(L_i) \simeq \frac{4e^2}{\pi h} - \alpha \frac{2e^2}{h} \mathrm{Log}\left(\frac{L_i}{L_e}\right) . \qquad (16)$$

The coefficient is $\alpha \simeq 0.25$. Here we give additional results as compared to the main text. Figure 7 shows the results for $\sigma(L_i)$ for 0.2% of resonant adsorbates in a series of energies chosen in the region of the plateau (see figure 6). One sees that the variation of conductivity is in agreement with equation (16) except for the lowest energy $E = 0.01\,\mathrm{eV}$ and the highest $E > 0.1\,\mathrm{eV}$. Indeed these energies mark the lower bound and upper bound of the intermediate regime. We have checked that this law

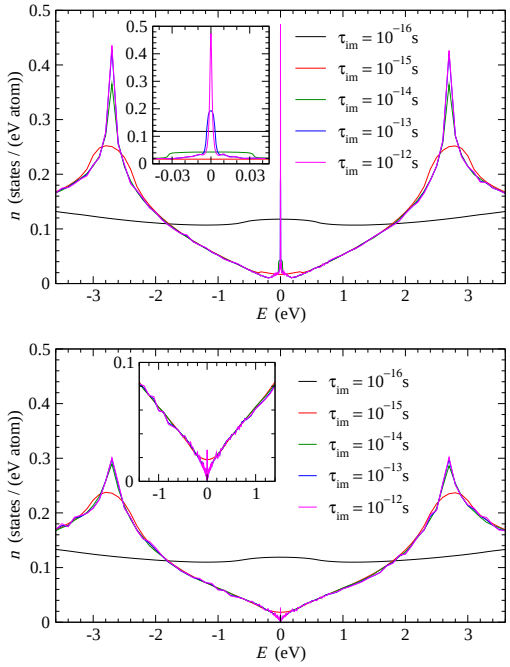

FIG. 9: Density of states $\langle n(E)\rangle_\eta$ versus energy E for various values of mixing energy $\delta E = \hbar/\tau_{im} = \eta\hbar/\tau_i$ (see text). Upper panel: Concentration 0.4% of resonant adsorbates (monovacancies). Lower panel: Concentration 2% of non resonant adsorbates (divacancies). At this concentration small clusters of adsorbates exist that create a peak in the density of states. This peak exists only for sufficiently long inelastic scattering time.

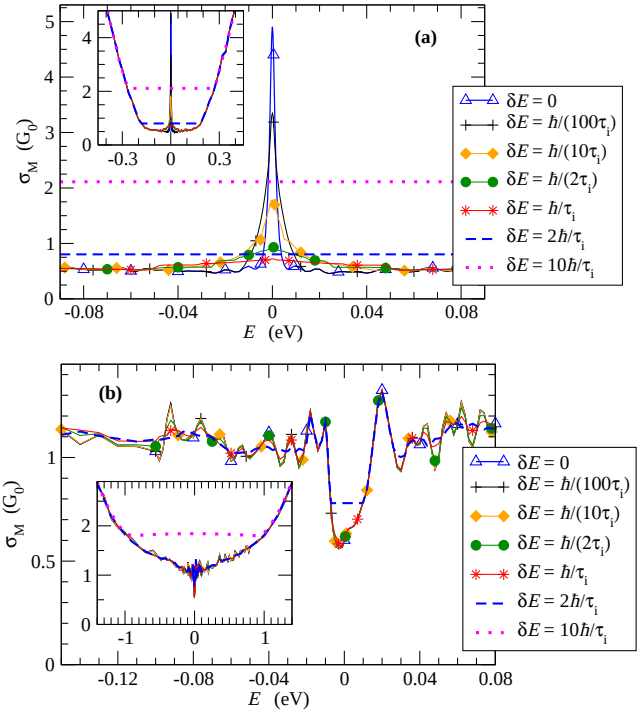

FIG. 10: Microscopic conductivity $\langle\sigma_M(E)\rangle_\eta$ in unit of $G_0 = 2e^2/h$ versus energy E, for various values of the mixing energy δE, corresponding to η varying from 1/100 to 10 (see text). (a) Concentration 0.4% of Resonant adsorbates (monovacancies). (b) Concentration 2% of non resonant adsorbates (divacancies).

(equation (16)) is valid even at higher concentration up to 10% of monovacancies (figure 8).

V. EFFECT OF THE MIXING OF STATES INDUCED BY THE INELASTIC SCATTERING

In the presence of inelastic scattering the long time propagation becomes diffusive as explained in the main text and in the second section of this supplementary material. However there is another effect of the inelastic scattering. Indeed due to this scattering the eigenstates of the static Hamiltonian are no more eigenstates of the real system. Typically one expects that states in the energy range $E_F \pm \delta E/2$ with $\delta E = \eta\hbar/\tau_i$ are mixing. $\eta = \tau_i/\tau_{im}$ is the ratio between the cutoff time τ_i of the weak localization (dephasing time) and the inelastic scattering time τ_{im} corresponding to mixing of the DOS. If the density of states and the diffusivity change quickly with energy this effect may be important. η can depend on the system under consideration and we have at present no way to estimate it exactly. Therefore we analyze this effect by computing the average of the density of states and of the conductivity in the energy window $E_F \pm \delta E/2$ with $\delta E = \eta\hbar/\tau_i$ with η varying from 1/100 to 10,

$$\langle n(E)\rangle_\eta = \frac{1}{\delta E}\int_{E-\delta E/2}^{E+\delta E/2} n(u)\mathrm{d}u\,, \qquad (17)$$

$$\langle \sigma(E,\tau_i)\rangle_\eta = \frac{1}{\delta E}\int_{E-\delta E/2}^{E+\delta E/2} \sigma(u,\tau_i)\mathrm{d}u\,. \qquad (18)$$

We find that this effect plays a minor role except for resonant adsorbates with strong inelastic scattering and very close to the Dirac energy where both the density of states and the microscopic conductivity are modified by the mixing of states (see figures 9 and 10). As shown in figures 11 and 12 the long time regime which manifests the effect of Anderson localization is insensitive to the effect of mixing of states.

[1] C. Berger, Z. Song, T. Li, X. Li, A. Y. Ogbazghi, R. Feng, Z. Dai, A. N. Marchenkov, E. H. Conrad, P. N. First, and W. A. de Heer, *Ultrathin Epitaxial Graphite: 2D Electron Gas Properties and a Route toward Graphene-based Nanoelectronics*, J. Phys. Chem. B **108**, 19912 (2004).

[2] K. S. Novoselov, A. K. Geim, S. V. Morozov, D. Jiang, M. I. Katsnelson, I. V. Grigorieva, S. V. Dubonos, and A. A.

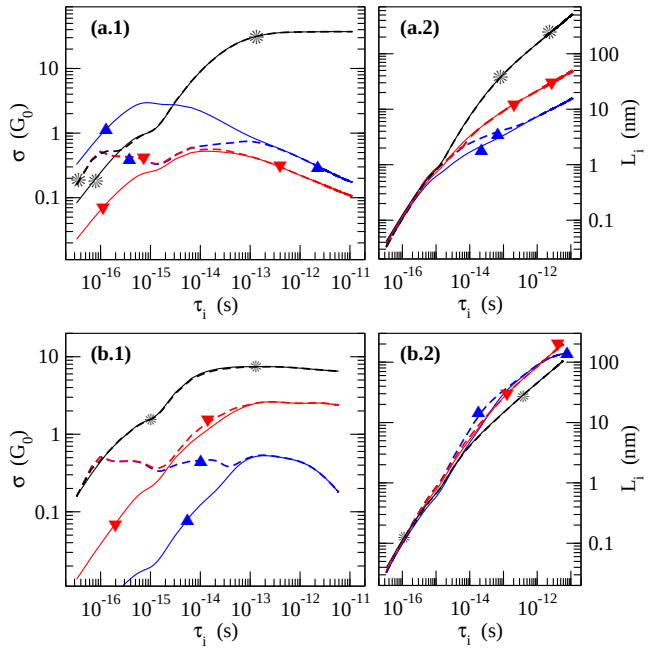

FIG. 11: Conductivity $\sigma(E,\tau_i)$ and inelastic mean-free path $L_i(E,\tau_i)$ versus inelastic scattering time τ_i. Same concentrations and energies as in figure 6. (a) Concentration 0.2% of resonant adsorbates (monovacancies) for energies $E = 0$ (triangle up), $E = 0.04\,\text{eV}$ (triangle down) and $E = 0.8\,\text{eV}$ (star). (b) Concentration 1% of non resonant adsorbates (divacancies) for energies $E = 0$ (triangle up), $E = 0.1\,\text{eV}$ (triangle down) and $E = 1.5\,\text{eV}$ (star). (Lines) without mixing on energy, (dashed lines) with mixing on an energy range $\delta E = \hbar/\tau_i$, i.e. $\eta = 1$ (see text). $G_0 = 2e^2/h$.

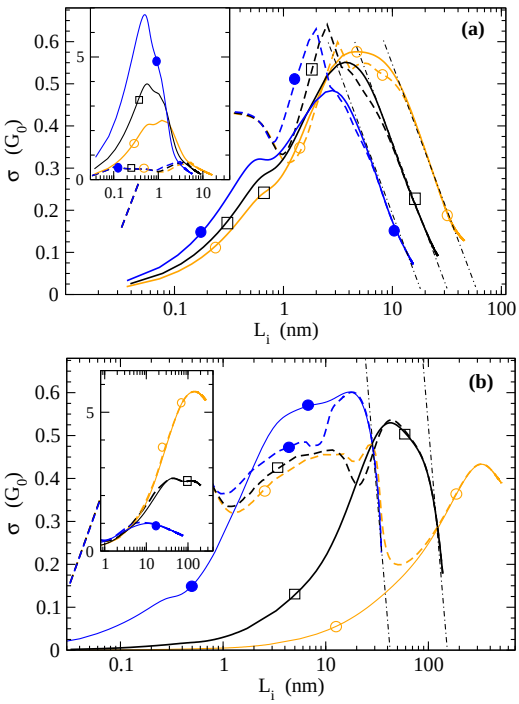

FIG. 12: Conductivity σ in units of $G_0 = 2e^2/h$ as a function of inelastic scattering length L_i for the 3 concentrations of adsorbates (with the same symbols as in the main text figures 2(b) and 4(b)). (a) resonant adsorbates (monovacancies) at energies $E = 0.03\,\text{eV}$. (b) non resonant adsorbates (divacancies) at $E = 0\,\text{eV}$. (Continuous lines) with $\delta E = 0$, (dashed lines) with $\delta E = \hbar/\tau_i$, i.e. $\eta = 1$ (see text). The dot-dashed straight lines show the slope $-\alpha$ for $L_i \gg L_e$ (equation (4)): (a) $\alpha = 0.25$ and (b) $\alpha = 0.75$. The inset shows (a) $\sigma(L_i)$ at $E = 0$ and (b) $\sigma(L_i)$ at $E = 0.1\,\text{eV}$.

Firsov, *Two-dimensional gas of massless Dirac fermions in graphene*, Nature, **438**, 197 (2005).

[3] Y. Zhang, Y.-W. Tan, H. L. Stormer, and P. Kim, *Experimental observation of the quantum Hall effect and Berrys phase in graphene*, Nature, **438**, 201 (2005).

[4] C. Berger, Z. Song, X. Li, X. Wu, N. Brown, C. Naud, D. Mayou, T. Li, J. Hass, A. N. Marchenkov, E. H. Conrad, P. N. First, and W. A. de Heer, *Electronic confinement and coherence in patterned epitaxial graphene*, Science, **312**, 1191 (2006).

[5] A. Hashimoto, K. Suenaga, A. Gloter, K. Urita, and S. Iijima, *Direct evidence for atomic defects in graphene layers*, Nature **430**, 870 (2004).

[6] X. Wu, X. Li, Z. Song, C. Berger, and W. A. de Heer, *Weak antilocalization in epitaxial graphene: Evidence for chiral electrons*, Phys. Rev. Lett. **98**, 136801 (2007).

[7] X. Wu, M. Sprinkle, X. Li, F. Ming, C. Berger, and W. A. de Heer, *Epitaxial-graphene/graphene-oxide junction: An essential step towards epi- taxial graphene electronics*, Phys. Rev. Lett. **101**, 026801 (2008).

[8] S. Y. Zhou, D. A. Siegel, A. V. Fedorov, and A. Lanzara, *Metal to insulator transition in epitaxial graphene induced by molecular doping*, Phys. Rev. Lett. **101**, 086402 (2008).

[9] R. Grassi, T. Low, and M. Lundstrom, *Metal to insulator transition in epitaxial graphene induced by molecular doping*, Nano. Lett. **11**, 4574 (2011).

[10] N. M. R. Peres, F. Guinea, and A. H. Castro Neto, *Electronic properties of disordered two-dimensional carbon*, Phys. Rev. B **73**, 125411 (2006).

[11] A. Bostwick, J. L. McChesney, K. V. Emtsev, T. Seyller, K. Horn, S. D. Kevan, and E. Rotenberg, *Quasiparticle Transformation during a Metal-Insulator Transition in Graphene*, Phys. Rev. Lett. **103**, 056404 (2009).

[12] X. Wu, X. Li, Z. Song, C. Berger, and W. A. de Heer, *Weak antilocalization in epitaxial graphene: Evidence for chiral electrons*, Phys. Rev. Lett. **102**, 236805 (2009).

[13] N. Leconte, J. Moser, P. Ordejon, H. Tao, A. Lherbier, A. Bachtold, F. Alsina, C. M. Sotomayor Torres, J.-C. Charlier, and S. Roche, *Damaging graphene with ozone treatment: A chemically tunable metal insulator transition*, ACS Nano **4**, 4033 (2010).

[14] S. Roche, N. Leconte, F. Ortmann, A. Lherbier, D. Soriano, and J.-C. Charlier, *Quantum transport in disordered graphene: A theoretical perspective*, Solid States Comm. **152**, 1404 (2012).

[15] T. Fukuzawa, M. Koshino, and T.Ando, *Weak-Field Hall Eect in Graphene Calculated within Self-Consistent Born Approximation*, J. Phys. Soc. Jpn. **78**, 094714 (2009).

[16] F. Guinea, *Models of Electron Transport in Single Layer Graphene*, J. Low Temp. Phys. **153**, 359 (2008).

[17] V. M. Pereira, J. M. B. Lopes dos Santos, and A. H.

Castro Neto, *Modeling disorder in graphene*, Phys. Rev. B **77**, 115109 (2008).
[18] J. P. Robinson, H. Schomerus, L. Oroszlany, and V. I. Falko, *Adsorbate-Limited Conductivity of Graphene*, Phys. Rev. Lett. **101**, 196803 (2008).
[19] T. O. Wehling, S. Yuan, A. I. Lichtenstein, A. K. Geim, and M. I. Katsnelson, *Resonant Scattering by Realistic Impurities in Graphene*, Phys. Rev. Lett. **105**, 056802, (2010).
[20] Y. V. Skrypnyk and V. M. Loktev, *Electrical conductivity in graphene with point defects*, Phys. Rev. B. **82**, 085436 (2010).
[21] Y. V. Skrypnyk and V. M. Loktev, Phys. Rev. B. **83**, 085421 (2011).
[22] A. Ferreira et al., Phys. Rev. B **83**, 165402 (2011).
[23] P. M. Ostrovsky et al., Phys. Rev. Lett. **105**, 266803 (2010).
[24] J. Bang and K. J. Chang, *Localization and one-parameter scaling in hydrogenated graphene* Phys. Rev. B **81**, 193412 (2010).
[25] N. M. R. Peres, *The transport properties of graphene*, Journal of Physics: Condensed Matter **21** (2009) 323201.
[26] V. M. Pereira, F. Guinea, J. M. B. Lopes dos Santos, N. M. R. Peres, and A. H. Castro Neto, *Disorder induced localized states in graphene*, Phys. Rev. Lett. **110**, 196601 (2013).
[27] V. M. Pereira, F. Guinea, J. M. B. Lopes dos Santos, N. M. R. Peres, and A. H. Castro Neto, *Disorder induced localized states in graphene*, Phys. Rev. Lett. **96**, 036801 (2006).
[28] A. Incze, A. Pasturel and C. Chatillon, *Oxidation of graphite by atomic oxygen: a first-principles approach*, Surface Science **537**, 55 (2003).
[29] A. Lherbier et al., A. Lherbier, S. M.-M. Dubois, X. Declerck, Y.-M. Niquet, S. Roche, and J.-C. Charlier, *Transport properties of graphene containing structural defects*, Phys. Rev. B **86**, 075402 (2012).
[30] R. R. Nair, M. Sepioni, I.-L. Tsai, O. Lehtinen, J. Keinonen, A. V. Krasheninnikov, T. Thomson, A. K. Geim, and I. V. Grigorieva, *Spin-half paramagnetism in graphene induced by point defects*, Nature Phys. **8**, 199 (2012).
[31] D. Mayou, *Calculation of the conductivity in the short-mean-free-path regime*, Europhys. Lett. **6**, 549 (1988).
[32] D. Mayou and S. N. Khanna, *A Real-Space Approach to Electronic Transport*, J. Phys. I Paris **5**, 1199 (1995).
[33] S. Roche and D. Mayou, *Conductivity of quasiperiodic systems: A numerical study*, Phys. Rev. Lett. **79**, 2518 (1997).
[34] S. Roche and D. Mayou, *Formalism for the computation of the RKKY interaction in aperiodic systems*, Phys. Rev. B **60**, 322 (1999).
[35] F. Triozon, Julien Vidal, R. Mosseri, and D. Mayou, *Quantum dynamics in two- and three-dimensional quasiperiodic tilings*, Phys. Rev. B **65**, 220202 (2002).
[36] A. Lherbier, B. Biel, Y.-M. Niquet, and S. Roche, *Transport length scales in disordered graphene-based materials: Strong localization regimes and dimensionality effects*, Phys. Rev. Lett. **100**, 036803 (2008).
[37] A. Lherbier, X. Blase, Y.-M. Niquet, F. Triozon, and S. Roche, *Charge transport in chemically doped 2d graphene*, Phys. Rev. Lett. **101**, 036808 (2008).
[38] G. Trambly de Laissardière and D. Mayou *Electronic transport in Graphene: Quantum effects and role of loacl defects*, Mod. Phys. Lett. B, **25** 1019, (2011).
[39] N. Leconte, A. Lherbier, F. Varchon, P. Ordejon, S. Roche, and J.-C. Charlier, *Quantum transport in chemically modied two-dimensional graphene: From minimal conductivity to Anderson localization*, *Phys. Rev. B* **84**, 235420 (2011).
[40] A. Lherbier, S. M.-M. Dubois, X. Declerck, S. Roche, Y.-M. Niquet, and J.-C. Charlier, *Two-dimensional graphene with structural defects: Elastic mean free path, minimum conductivity and anderson transition*, Phys. Rev. Lett. **106**, 046803 (2011).
[41] N. Leconte, D. Soriano, S. Roche, P. Ordejon, J.-C. Charlier, and J. J. Palacios, *Magnetism-Dependent Transport Phenomena in Hydrogenated Graphene: From Spin-Splitting to Localization Eects*, ACS Nano **5**, 3987 (2011).
[42] G. Trambly de Laissardière, J.-P. Julien, and D. Mayou, *Quantum transport of slow charge carriers in quasicrystals and correlated systems*, Phys. Rev. Lett. **97**, 026601 (2006).
[43] C. Berger, E. Belin, and D. Mayou, *Electronic properties of Quasi-crystals*, Ann. Chim. Mater. (Paris), **18**, 485 (1993).
[44] E. Belin and D. Mayou, *Electronic properties of Quasicrystals*, Phys. Scr., **T49A**, 356 (1993).
[45] G. Trambly de Laissardière, D. Nguyens-Manh, and D. Mayou, *Electronic structure of complex Hume-Rothery phases and quasicrystals in transition metal aluminides*, Prog. Mater. Sci., **50**, 679 (2005)
[46] D. Mayou, *Generalized Drude Formula for the Optical Conductivity of Quasicrystals*, Phys. Rev. Lett. **85**, 1290 (2000).
[47] S. Ciuchi, S. Fratini, and D. Mayou, *Transient localization in crystalline organic semiconductors*, Phys. Rev. B **83**, 081202(R) (2011).
[48] P. A. Lee and T. V. Ramakrishnan, *Disordered electronic systems*, Rev. Mod. Phys. **57**, 287 (1985).
[49] E. McCann, K. Kechedzhi, V. I. Falko, H. Suzuura, T. Ando, and B. L. Altshuler, *Weak-Localization Magnetoresistance and Valley Symmetry in Graphene*, Phys. Rev. Lett. **97**, 146805 (2006).
[50] E. R. Mucciolo and C. H. Lewenkopf, *Disorder and electronic transport in graphene*, J. Phys.: Cond. Matter **22**, 273201 (2010).
[51] S. Nakaharai, T. Iijima, S. Ogawa, S. Suzuki, S.-L. Li, K. Tsukagoshi, S. Sato, and N. Yokoyama, *Conduction Tuning of Graphene Based on Defect-Induced Localization*, ACS Nano **7**, 5694 (2013).
[52] F. Ducastelle, *Electronic structure of vacancy resonant states in graphene: a critical review of the single vacancy case*, CondMat. arXiv:1305.2690 (2013).
[53] D. Mayou and G. Trambly de Laissardière, *Quantum transport in quasicrystlas and complex metallic alloys*, in Quasicrystals, series "Handbook of Metal Physics", editors T. Fujiwara, Y. Ishii (Elsevier, Amsterdam, 2008) p. 209-265.